A neural substrate for negative affect dictates parental behaviour

Salvatore Lecca
University of Lausanne
Mauro Congiu
Neuroscience Institute, Section of Cagliari, National Research Council , Cagliari
Lea Royon
The University of Lausanne
Leonardo Restivo
https://orcid.org/0000-0002-3709-5504
Benoit Girard
IGF-CNRS-UMR5203-INSERM-U661-UMI-II https://orcid.org/0000-0002-3914-6483
Noemie Mazare
The University of Lausanne
Camilla Bellone
Department of Fundamental Neuroscience, CMU, University of Geneva, Geneva, Switzerland.
https://orcid.org/0000-0002-6774-6275
Ludovic Telley
University of Lausanne https://orcid.org/0000-0002-5041-1997
Manuel Mameli (manuel.mameli@unil.ch)
The University of Lausanne https://orcid.org/0000-0002-0570-6964

Article

Keywords:

Posted Date: April 15th, 2022

DOI: https://doi.org/10.21203/rs.3.rs-1461765/v1

Abstract

Parental behaviours are essential to secure survival and wellbeing of newborns1. Concomitantly, parenting also limits negative affective states in adults, which emerge when the coping with excessive neonatal distress becomes a challenge1–5. Whether neural circuits that process negative affect orchestrate components of parental behaviours remains, however, unknown. Here, we identify functional and transcriptional signatures of parental behaviours in neurons of the negative emotion center lateral habenula receiving bed nucleus of the stria terminalis innervation (BNSTLHb). Calcium imaging reveals that LHb neurons of virgin female mice increase their activity during pup retrieval to a nest, a behaviour that disappears following optogenetic LHb inactivation. Intersectional cell identification and transcriptional profiling of BNSTLHb neurons associates this neuronal population to parental behaviours and outlines gene expression in female virgins that is similar to mothers but divergent from virgin males. From a functional standpoint, optogenetic activation and inactivation of the BNSTLHb pathway maximizes and suppresses, respectively, the parental behaviour. Finally, tracking of single BNSTLHb cell activity demonstrates specificity of this neuronal subset for encoding negative stimuli and pup retrieval, but not sociability amongst conspecifics. Thus, BNSTLHb cells are operational for female parenting, demonstrating that neural circuit elements for negative affect contribute to specific social interactions.

Main

Virgin and sexually-experienced female mice show parental behaviours including retrieval of a distressed pup from an open environment to a nest[1,6]. Notably, neonatal distress can also produce frustration and negative emotions that both humans[2,3] and rodents[1,4] intend to reduce through parental behaviours. Accordingly, female mice reinforce their behaviours to mute pup vocalization or reduce distressed pup body stretching[5,7]. Here we examine whether neural circuits processing negative affect contribute to parental behaviours.

The lateral habenula (LHb) is excited by aversive stimuli of diverse nature [8], and guides actions directed to avoid negative outcomes[9–11]. Notably, LHb lesioning impairs parental behaviours[12,13] suggesting that a yet unidentified, ethologically relevant, function of the LHb may be to shape actions to end the negative emotions individuals experience during adult-newborn interactions.

Parental virgin females express a comparable palette of caring behaviours as sexually-experienced female mice, rendering these actions independent from hormonal fluctuations typical of motherhood[14]. We took advantage from such a conserved phenotype, and examined parental behaviours in virgin female mice never exposed to pups by combining video-based monitoring and ultrasonic audio recordings (Fig. 1a,b and Extended Data Fig. 1a). Virgin female mice were placed in an arena and exposed to a series of novel foreign pups across multiple trials (pup zone, Fig. 1a). Pups laying in the pup zone displayed high vocalization and body movements as signs of distress[7] (Extended Data Fig. 1a,b). Each pup exposure (7–9 pups) terminated with either a failure (> 10 minutes/pup) or a pup retrieval to the nest. We then constructed ethograms and quantified the frequency and duration of each diverse

behaviours including nest building, pup grooming and pup retrieval[15,16] (Fig. 1b,c, Extended Data Fig. 1c–e, and Supplementary Video 1). Pup retrieval events occurred sporadically at the first pup exposure, with their probability increasing with subsequent pups[14] (Fig. 1d). Following successful retrieval, pups in the nest presented reduced vocalization and movements (Extended Data Fig. 1a,b). Thus, virgin female mice express parental behaviours, which lead to the reduction in pup distress[5,15].

To study LHb contribution to parental behaviours, we expressed GCaMP6f in the LHb of freely behaving virgin female mice and used fiber photometry[10,11] to monitor population calcium dynamics (Fig. 1e,f and Extended Data Fig. 1f). Pup retrieval events occurred along with a robust increase in LHb activity, which dropped when virgin females deposited pups into the nest (Fig. 1f). In contrast, such a raise in activity was not observed during grooming and nesting periods (Fig. 1f and Extended Data Fig. 1g). Fluorescent calcium transients lasted across entire pup retrieval events (9.3 ± 1.3 seconds), and their duration correlated with the length of pup retrievals (8.9 ± 1.2 seconds) (Fig. 1g). We thereby broke down pup retrieval instances into four sub-modules: *i.* pup approach, (with mice showing head direction to pups), *ii.* pup interaction, (when nose–body interaction occurs between virgin female and pup), *iii.* retrieval onset, (when pup–picking occurs) and *iv.* retrieval offset (with the pup deposited into the nest) (Fig. 1h). Fluorescence transients rose in LHb at pup interaction and terminated at pup retrieval offset (Fig. 1h). In contrast, activity remained unaffected when a virgin female interacted with a conspecific, an object or a pup in the nest, supporting a relationship between LHb activity and retrieval of a newborn in discomfort (Extended Data Fig. 1h). The increased LHb neuronal activity was causative for pup retrieval events in virgin female mice, as bilateral LHb inhibition with an inhibitory opsin (Jaws, time-locked with the entry of the female in the pup zone)[10] suppressed this behaviour (Fig. 1j). Light-driven LHb inactivation left intact grooming and locomotion, while reducing nest building. The latter may be either a consequence of impaired pup retrieval during LHb inhibition or indicative for a broader contribution of LHb to multiple parental actions (Extended Data Fig. 2c–e). Thus, neuronal excitation in LHb guides pup retrieval in virgin female mice.

Genetic and anatomical diversity in LHb infer cell-specific behavioural functions[17,18]. Hence, we examined whether pup retrieval is orchestrated by discrete LHb neuronal subpopulations. In vivo microendoscopic imaging through GCaMP6f expression in LHb virgin female mice enabled resolution of somatic calcium dynamics from hundreds of LHb neurons (n = 493 cells)[9] (Fig. 2a,b, Extended Data Fig. 3a and Supplementary Video 2). Visualization, and calcium signal tracking during the behavioural task identified a subset of LHb neurons that increased fluorescence from pup interaction to pup retrieval offset, matching the whole population activity dynamics (Fig. 1h, Fig. 2c,d). Clustering analysis algorithm identified two segregated neuronal clusters. While Cluster I lacked time-locked modulation of calcium signal during parental behaviours, increased neuronal activity during pup retrieval was restricted to Cluster II cells (Fig. 2e–f and Extended Data Fig. 3b–e). This suggests that LHb neurons participating in pup retrieval are functionally segregated. Remarkably, interaction with a conspecific did not change LHb activity, while object interaction and aversive airpuff increased fluorescence dynamics of a wide LHb neuronal population, including that of Cluster II neurons (Fig. 2f and Extended Data Fig. 3c–e). This

indicates specificity of Cluster II LHb neurons in encoding parental, but not other social behaviours. Next, we matched all fields of view (FOV) of GCaMP6f-expressing neurons with the respective Gradient Index (GRIN) lens borders and LHb anatomy (See methods). This unraveled that pup retrieval-activated neurons overlayed within the medial territory of the LHb (Fig. 2g,h and Extended Fig. 4a,b). Thus, pup retrieval recruits an aversive-responsive and medially-located LHb neuronal population[19].

Synaptic inputs emerging from the ventral pallidum, the medial septum and the bed nucleus of the stria terminalis (BNST) impinge onto and control the activity of medially-located LHb neurons[10,19]. Notably, the BNST senses hormonal changes, infant stimuli and its lesioning impairs parental behaviours[6,20]. Thus, we hypothesized that medially-located and pup retrieval-activated LHb cells are defined by BNST innervation (^{BNST}LHb). To label such a neuronal subset, we first injected a high-titer AAV1-Cre within the BNST to obtain anterograde transsynaptic expression of Cre recombinase. We concomitantly provided a Cre-dependent viral construct for the expression of GFP in the LHb (Fig. 3a)[21]. This approach labeled, for the vast majority, LHb neurons located in the medial territory (Fig. 3a,b).

Single cell transcriptomics identifies molecularly distinct LHb neurons according to their territorial distribution[17,18]. Hence, we first tested whether a parental transcriptional signature exists in ^{BNST}LHb cells from virgin female mice. Transsynaptic Cre-dependent recombination of a nuclear envelope-targeted GFP in the LHb (KASH-GFP)[22] enabled nuclear fluorescence-assisted cell sorting (FACS) and high-throughput single-nucleus transcriptional profiling of ^{BNST}LHb neurons in virgin females (Fig. 3c). Analysis of cellular transcriptional identities using Uniform Manifold Approximation and Projection (UMAP) reduction algorithm and graph-based clustering[23] revealed two transcriptionally distinct ^{BNST}LHb populations (A and B, Fig. 3d). Indicative of correct LHb cells targeting was the presence in both clusters of LHb-enriched genes including *Slc17a6*, *Gap43*, *Pdh10*, and *Htr2c* obtained through Differentially Expressed Genes (DEGs) analysis[17,18] (Fig. 3d,e and Supplementary Table 1). Cell-type label transfer analysis[23] revealed that clusters A and B correspond to LHb neurons molecularly matching those located in the medial territory (Extended Data Fig. 5c,d)[17,18]. Gene ontology analysis[24] highlighted “biological processes” containing the term “behaviour” for both clusters (Extended Data Fig. 5d), with enrichment of genes participating to hormonal processes, social and maternal behaviour selectively found in Cluster A[1,16] (Fig. 3f and Extended Data Fig. 5d). Thus, the ^{BNST}LHb neurons transcriptional features assign this neuronal population to parental processes.

Stereotyped parental behaviours are opposite based on gender: virgin and sexually-experienced females display parental behaviours, whereas virgin males typically attack pups (Fig. 1b–d)[25]. To corroborate the relevance of ^{BNST}LHb in parenting, we examined whether their transcriptome from virgin females matches that of sexually-experienced females (mothers) and diverges from that of virgin male mice. We labeled, isolated and sequenced ^{BNST}LHb neurons from female mothers that recently gave birth, as well as virgin males age-matched to virgin females previously analyzed (Fig. 3g). Label transfer confirmed the LHb identity in males and female mothers (Extended Data Fig. 6a). Graph-based cluster analysis recapitulated two main clusters across the three experimental groups and revealed a Cluster A subcluster (cluster A1)

segregated between females (virgin and mothers) and virgin male-derived neurons (Fig. 3h). Indeed, DEGs were identified between females (mothers and virgins) and virgin males for cluster A1 cells (Fig. 3i, Supplementary Table 2). Thus, gender determines independent parental transcriptional programs in ^{BNST}LHb neurons, prompting to investigate whether this neuronal subset supports both parenting and the encoding negative affect.

To functionally probe whether ^{BNST}LHb neurons are a substrate for pup retrieval, we first delineated BNST-to-LHb projections properties and their contribution to parenting behaviour. The expression of Channelrhodopsin-2 (ChR2) in the BNST and optical activation of BNST axons (473 nm) evoked excitatory postsynaptic responses and efficiently excited medial LHb neurons[10] (Extended Data Fig. 7a–d). ^{BNST}LHb cells increased their activity in response to aversive footshocks, implicating this neuronal subset in negative affect-encoding (Extended Data Fig. 7e,f). Finally, ChR2-assisted activation of BNST axons within the LHb promoted rapid and reliable pup retrieval, while Jaws-mediated silencing of the BNST-to-LHb projection suppressed pup retrieval, and reduced nesting (Fig. 4a–d, Extended Data Fig. 8a–f, Supplementary Video 3). Hence, BNST projections i. excite LHb cells responding to negative stimuli and ii. are necessary and sufficient for pup retrieval in virgin female mice.

To precisely monitor the function of ^{BNST}LHb neurons during parental behaviours, we combined AAV1-Cre-driven GCaMP6f expression with fiber photometry (Extended Fig. 9a,b). Fluorescent signal was stable during nest building and grooming, while augmented during pup interaction and retrieval onset (Extended Fig. 9c,d). In contrast, fluorescence remained unchanged in a complementary non-BNST receiving LHb neuronal population during retrieval (CreOff; Extended Data Fig. 9e–h, see Methods)[26]. Thus, neurons receiving BNST innervation are unique in the LHb to signal parental information. To further assess the contribution of ^{BNST}LHb neurons to pup retrieval, microendoscopic calcium imaging allowed recording of activity from this identified neuronal population (Fig. 4e and Extended Data Fig. 10a). A large fraction of ^{BNST}LHb neurons (~ 60%) increased their activity during pup interaction, retrieval onset and airpuff, but not grooming and nest building (Fig. 4f and Extended Data Fig. 10b–e). In support of a model whereby ^{BNST}LHb neuron activity encodes pup retrieval, a trial-by-trial decoding algorithm revealed active neurons of Cluster II and ^{BNST}LHb overlapping but diverging from Cluster I (Fig. 4g). Additionally, activity dynamics predicted pup interaction, retrieval onset as well as negative stimuli like airpuff (Fig. 4h and Extended Data Fig. 10e,f). This corroborated the high fidelity of responses in Cluster II and ^{BNST}LHb neurons during interaction and onset of pup retrieval (Fig. 4h). Altogether, a select class of LHb neurons in the medial territory and innervated by BNST axons in virgin female mice defines the contribution of a neural circuit for negative affect in parental behaviours.

The capacity to rapidly operate parental behaviours (in non-parents and parents) that benefit a distressed infant has fundamental implications for the physical and emotional welfare of newborns. Alongside, a distressed neonate also spurs parental behaviours that limit the emergence of negative emotions in adults[1,2,4,5,7]. However, whether parental behaviours also recruit neural circuits processing negative affect has rarely been studied[1,16]. Our current findings suggests that BNST projections to the LHb primarily

control medially-located cells to drive pup retrieval. Vomeronasal, auditory cortex and medial preoptic area neurons (MPOA) are instrumental for parenting[1]. The MPOA, in turn, governs a complex network of downstream brain structures including BNST and LHb[16]. Whether each anatomical module serves for unique encoding (i.e. auditory calls, pup temperature, internal state) and how each integrates within the parenting neural system[1] remains elusive. Yet our results are unprecedented in delineating a brain network for negative affect contributing to the nurturing of newborns.

The transcriptionally shared molecular signatures of ^{BNST}LHb cells between virgin and mother female mice (as opposed to virgin males) provide a rich library to study biologically meaningful factors contributing to parenting. Our data identify a universal genetic program in females, independent of sexual or motherhood experience, and reveals transcriptomic features likely at the basis of the divergent parental strategies deployed by female and male individuals[16–18]. In contrast to females, male mice transition from pup aggression to parenting after mating[27]. Whether ^{BNST}LHb neurons undergo genetic, functional or circuit adaptations in male mice to enable this behavioural shift remains an open question. Our identification of differential expression in neuromodulatory (*Hcrt2*), protein adhesion (*Epha5*), and synaptic (*Gabra2*) components emerging in ^{BNST}LHb neurons across genders offers testable targets to address these questions.

Traumatic experience hampers LHb function, compromises BNST synaptic excitation onto the LHb[10] and impairs LHb neuronal activity[28,29] consequently favoring the establishment of pathological negative states[19]. Considering the vulnerability of parental behaviours to traumas and environmental stressors[30] our study offers a neural framework to understand disrupted adult-newborn relationships, including those occurring during postpartum depression.

References

1. Dulac, C., O'Connell, L. A. & Wu, Z. Neural control of maternal and paternal behaviors. Science **345**, 765–770 (2014).
2. Barr, R. G. Preventing abusive head trauma resulting from a failure of normal interaction between infants and their caregivers. Proc Natl Acad Sci U S A **109 Suppl 2**, 17294–17301 (2012).
3. Gustafson, G. E. & Green, J. A. On the importance of fundamental frequency and other acoustic features in cry perception and infant development. Child Dev **60**, 772–780 (1989).
4. Rosenblatt, J. S. Nonhormonal basis of maternal behavior in the rat. Science **156**, 1512–1514 (1967).
5. Schiavo, J. K. et al. Innate and plastic mechanisms for maternal behaviour in auditory cortex. Nature **587**, 426–431 (2020).
6. Numan, M. A lesion and neuroanatomical tract-tracing analysis of the role of the bed nucleus of the stria terminalis in retrieval behavior and other aspects of maternal responsiveness in rats. Dev Psychobiol **29**, 23–51 (1996).

7. Esposito, G. et al. Infant calming responses during maternal carrying in humans and mice. Curr Biol **23**, 739–745 (2013).
8. Matsumoto, M. & Hikosaka, O. Lateral habenula as a source of negative reward signals in dopamine neurons. Nature **447**, 1111–1115 (2007).
9. Lecca, S. et al. Heterogeneous Habenular Neuronal Ensembles during Selection of Defensive Behaviors. Cell Rep **31**, 107752 (2020).
10. Nuno-Perez, A. et al. Stress undermines reward-guided cognitive performance through synaptic depression in the lateral habenula. Neuron **109**, 947–956.e5 (2021).
11. Trusel, M. et al. Punishment-Predictive Cues Guide Avoidance through Potentiation of Hypothalamus-to-Habenula Synapses. Neuron **102**, 120–127.e4 (2019).
12. Corodimas, K. P., Rosenblatt, J. S., Canfield, M. E. & Morrell, J. I. Neurons in the lateral subdivision of the habenular complex mediate the hormonal onset of maternal behavior in rats. Behav Neurosci **107**, 827–843 (1993).
13. Felton, T. M., Linton, L., Rosenblatt, J. S. & Morrell, J. I. Intact neurons of the lateral habenular nucleus are necessary for the nonhormonal, pup-mediated display of maternal behavior in sensitized virgin female rats. Behav Neurosci **112**, 1458–1465 (1998).
14. Stolzenberg, D. S. & Rissman, E. F. Oestrogen-independent, experience-induced maternal behaviour in female mice. J Neuroendocrinol **23**, 345–354 (2011).
15. Carcea, I. et al. Oxytocin neurons enable social transmission of maternal behaviour. Nature **596**, 553–557 (2021).
16. Kohl, J. Parenting - a paradigm for investigating the neural circuit basis of behavior. Curr Opin Neurobiol **60**, 84–91 (2020).
17. Hashikawa, Y. et al. Transcriptional and Spatial Resolution of Cell Types in the Mammalian Habenula. Neuron **106**, 743–758.e5 (2020).
18. Wallace, M. L. et al. Anatomical and single-cell transcriptional profiling of the murine habenular complex. Elife **9**, (2020).
19. Hu, H., Cui, Y. & Yang, Y. Circuits and functions of the lateral habenula in health and in disease. Nat Rev Neurosci **21**, 277–295 (2020).
20. McHenry, J. A., Rubinow, D. R. & Stuber, G. D. Maternally responsive neurons in the bed nucleus of the stria terminalis and medial preoptic area: Putative circuits for regulating anxiety and reward. Front Neuroendocrinol **38**, 65–72 (2015).
21. Zingg, B. et al. AAV-Mediated Anterograde Transsynaptic Tagging: Mapping Corticocollicular Input-Defined Neural Pathways for Defense Behaviors. Neuron **93**, 33–47 (2017).
22. Swiech, L. et al. In vivo interrogation of gene function in the mammalian brain using CRISPR-Cas9. Nat Biotechnol **33**, 102–106 (2015).
23. Hao, Y. et al. Integrated analysis of multimodal single-cell data. Cell **184**, 3573–3587.e29 (2021).

24. Subramanian, A. et al. Gene set enrichment analysis: a knowledge-based approach for interpreting genome-wide expression profiles. Proc Natl Acad Sci U S A **102**, 15545–15550 (2005).
25. Lonstein, J. S. & De Vries, G. J. Sex differences in the parental behavior of rodents. Neurosci Biobehav Rev **24**, 669–686 (2000).
26. Saunders, A. & Sabatini, B. L. Cre Activated and Inactivated Recombinant Adeno-Associated Viral Vectors for Neuronal Anatomical Tracing or Activity Manipulation. *Curr Protoc Neurosci* **72**, 1.24.1–1.24.15 (2015).
27. Isogai, Y. et al. Multisensory Logic of Infant-Directed Aggression by Males. Cell **175**, 1827–1841.e17 (2018).
28. Lecca, S. et al. Rescue of GABAB and GIRK function in the lateral habenula by protein phosphatase 2A inhibition ameliorates depression-like phenotypes in mice. Nat Med **22**, 254–261 (2016).
29. Li, B. et al. Synaptic potentiation onto habenula neurons in the learned helplessness model of depression. Nature **470**, 535–539 (2011).
30. Hillerer, K. M., Neumann, I. D. & Slattery, D. A. From stress to postpartum mood and anxiety disorders: how chronic peripartum stress can impair maternal adaptations. Neuroendocrinology **95**, 22–38 (2012).

Online Methods

Experimental subjects

C57BL/6J wild-type female and male mice of 8-18 weeks were used for this study (Janvier lab, France). Mice were housed in groups of three or four per cage with water and food ad libitum on a 12:12 h light cycle (lights on at 7 a.m.) in individually ventilated cages (IVC, Innovive, France). Stimulus pups (2-6 days old) were from donor C57BL/6J pairs. All procedures were conducted in compliance with the Swiss National Institutional Guidelines on animal experimentation and were approved by the canton of Vaud Cantonal Veterinary Office Committee for Animal Experimentation (Switzerland; License VD3171).

Viruses

rAAV-DJ/8/2-hSyn1-eGFP-WPRE (titer, 9.4 x 10^{12} vg.ml-1), rAAV-DJ/8/2-hSyn1-GCaMp6f-WPRE (titer: titer: 4.5 x 1012 vg.ml-1), rAAV8-hsyn-hChR2(H134R)-EYFP (titer: 6.4 x 10^{12} vg.ml-1), rAAV1/2-hCMV-chl-Cre (titer: 1 × 10^{13} vg.ml-1), rAAV-DJ/8/2-hSyn1-dlox-EGFP(rev)-dlox (titer: 6.4 x 10^{12} vg.ml-1), rAAV-DJ/8/2-hEF1α-dlox-GCaMP6f-lox-WPRE (titer: 4.5 x 10^{12} vg.ml-1), ssAAV-DJ/2-shortCAG-loxFAS-GCaMP6s-loxFAS-WP1RE-hGH (titer: 4.5 x 10^{12} vg.ml-1) were purchase from the UZH Vector Facility (Zurich, Switzerland). rAAV8-hSyn1-JAWS-GFP (titer: 1.3 x 1013 vg.ml-1) was purchased from Addgene. rAAV2.5-CAG-Flex-EGFP-KASH (titer 1.045 x 10^{13} vg.ml-1) aliquots were gently provided by Magdalena Gotz and Riccardo Bocchi (Biomedical Center, Ludwig-Maximilians-Universitatet).

Stereotaxic surgeries

Mice were anaesthetized with ketamine (150 mg/kg)/xylazine (10 mg/kg) (Cantonal University Hospital, Lausanne, Switzerland). The ocular protector Viscotear was used to prevent eye damage. The surgery was performed on a heating pad to keep a stable body temperature. When the mouse was deeply asleep, we performed a local anesthesia (subcutaneous injection) with a mix of lidocaïne (6mg/kg) and bupivacaine (2.5mg/kg). We then unilaterally injected in the LHb (−1.4 mm AP, 0.45 ML, 3.1 mm DV) GCaMP6f or flex-GCAMP6f or creoff-GCAMP6s using a glass pipette on a stereotactic frame (Kopf, France). For optogenetic and cell counting experiments, we bilaterally injected in the LHb the inhibitory opsin JAWS or eGFP virus or a flex eGFP or a eGFP KASH. For these injections volumes ranged between 150 and 250 nl. An anterograde transynaptic AAV1ht-CRE virus or JAWS or ChR2 or eGFP were injected unilaterally or bilaterally in the BNST (+0.24 mm AP, 0.85 mm ML, 4.5 mm DV) with a volume ranging between 50 to 150 nl. All injections were performed at a rate of approximately 100-150 nl/min. The injection pipette was withdrawn from the brain 10 minutes after the infusion. Animals were allowed to recover for a minimum of two weeks before fiber or GRIN lenses implantation.

Chronic implants

For fiber photometry experiments, a single fiber probe (200 µm, Chi Square Bioimaging) was placed and fixed (C and B Metabond, Parkell) 150 µm above the injection site in the LHb, lowered at a constant speed of 7 µm/s. For optogenetic manipulation a single fiber (200 µm, Thorlabs) was placed at the following coordinates from Bregma (AP: −1.4 mm, L: ± 0.1 mm, V: −2.6 mm from skull surface). Surgery was performed under isoflurane anesthesia (induction: 4%, maintenance: 1.8%–2%, Univentor).

For endoscope experiments, mice were anaesthetized (as described above) and implanted with a GRIN lens (6.1mm length, 0.5mm diameter; Inscopix, #100-000588). The lens was placed ∼150–200 µm above the injection site using the following coordinates: −1.40 mm posterior to bregma, 0.45 mm lateral from midline, and −2.85 to −2.9 mm ventral to skull surface (lowered at a speed of 1µm/s). For pain management, paracetamol (500mg/250ml; 200-300mg/kg/day) was added to the drinking water after the surgery. Two weeks after lens implantation, mice were again anaesthetized (isoflurane, as above) and a baseplate (Inscopix, #100- 000279) was secured above the lens. A doom micro-camera (Inscopix) was attached to the baseplate allowing efficient habituation of the mice to the micro-endoscope weight. The latter procedure ensure that mice display comparable behaviour with no implanted pairs during the recording session. Proper viral expression and fiber/GRIN lens placement in brain areas of interest were confirmed post hoc using histology for all experiments.

Histology, immunohistochemistry, and microscopy

For immunohistochemistry, mice were terminally anaesthetized with ketamine and xylazine and perfused transcardially with paraformaldehyde (PFA) 4% in 0.1 M phosphate buffered saline (PBS). Brains were collected and left overnight in 4% PFA at 4°C until slicing. Consecutive coronal slices (60 microns) of LHb and BNST were sectioned using a vibratome (Leica VT1200S). LHb slices were stained for NeuN, a neuron-specific nuclear marker, using a classical immunohistochemical protocol. Prior to immunostaining, slices were incubated in blocking buffer (10% Normal Goat Serum (NGS), 0.25% Triton

in PBS) for 1 hour. All antibodies were diluted in PBS with 0.25% Triton and 3% NGS. Neurons were stained with a mouse anti-NeuN primary antibody, (Millipore, dilution: 1/500) incubated 48h at 4°C. Following extensive rinses with PBS, slices were left overnight at 4°C with a goat anti-mouse secondary antibody coupled with the fluorescent protein Alexa 555 (Invitrogen, dilution 1/500). Slices were mounted on glass slides with FluorSave reagent. Images of the LHb (6 slices/mouse) were acquired using a confocal microscope (TCS SP5 AOBS TANDEM, Leica) with a 20X objective using the same acquisition parameters between mice. For the cell counting, we selected for each mouse (n=4) 6 slices (60microns) containing the LHb, at 3 different coordinates in the antero-posterior axis (AP: -1.3, -1.4, -1.5 mm from Bregma). For each slice, the LHb was divided into two sub regions, the lateral and the medial LHb. The number of eGFP and NeuN-positive neurons was counted using ImageJ Cell Counter plugin. We then plotted the ratio of GFP positive cells on the total cells (NeuN positive cells).

To validate injection site in the BNST, we performed a staining for the Cre recombinase protein, using a similar protocol mentioned earlier or we co-inject fluorescent beads dye. Slices were incubated in the mouse anti-Cre primary antibobody (Millipore, dilution 1/500) 24h at 4°C, and in the goat anti-mouse secondary antibody coupled with the fluorescent protein Alexa 555 (Invitrogen, dilution 1/500) 2h at room temperature. We took images of the BNST slices with an epi-fluorescent microscope (Zeiss).

Behavioural assays

Pup retrieval. Animals were placed in a phenotyper box (Noldus, 58cm H, 30cm L, 30cm W). In addition of the top view camera provided by the phenotyper, an extra phenotyper lid with the embedded camera was placed on the side of the arena ensuring a close video-recording of the behaviour with a lateral point of view. The arena was filled with standard wood chip bedding (Safe, Germany) and divided in 2 main zones (see Fig. 1a): a nest zone provided by nest material (paper Kleenex) and a pup zone (in the opposite corner) where the pup was placed through an external sliding door. Video recording was controlled with EthovisionXT 15 (Noldus Information Technology).

Mice underwent a period of habituation to the arena of 15-20 min every day for 2 consecutive days. For the experiment, after 5-10 min of acclimatization, we placed the pup in the pup zone until it was retrieved to the nest (10 min maximum). If the pup was not retrieved after the 10 min, it was replaced by another pup. If it was retrieved within the 10 min, another pup was immediately placed in the pup zone.

Pup calls recording and pup motion tracking. Two microphones (UltraVox XT, Noldus) allowing ultrasound vocalization (USVs) recordings were placed 16 cm above the pup zone and the nest zone, respectively. A pup was placed in the pup zone and the recording was acquired for 5 minutes. After, a virgin female (previously selected for its high retrieval score) was introduced to the arena and retrieved the pup to the nest (pups were retrieved within 2 minutes). Ten minutes later, the female was gently removed from the phenotyper and USVs were recorded through the microphone placed above the nest zone. The number of USVs call (40-90 KHz) was analyzed with the Ultravox CTsound software and plotted for the same pup in the 2 different conditions. The order of the procedure was inverted for 4 pups. Pup movements were tracked using Ethovision XT15 as follows: the pup was segmented from the

background using Ethovision's standard detection method (Dynamic Subtraction), the resulting area in pixel and how it changes across frames (threshold: change > 60% of the area) was used to estimate body movement and crawling.

Conspecific, object exposure and airpuff. Females employed for the photometry and endoscope experiments were also exposed to sessions (5 minutes each) with a conspecific (male C57BL6/J of 4 weeks old), an object (a falcon tube cap) or an unpredicted series of airpuffs (5, 500ms duration, 1.5 bar, randomly presented in 5 min).

Video recording was synchronized with the photometric and endoscopic aquisition using hardware-time signals controlled with a I/O box (Noldus).

Behavioural scoring

Automatic behavioural scoring was performed with Ethovision XT 15. For each mouse, speed, time spent in the zones, and mobility (displacement of the body center point > 2 cm/s) were collected from the video file. Manual behavioural annotation was performed on a frame-by-frame basis using the manual scoring module of EthovisionXT 15 or the video function of Spike2 (Cambridge Electronic Design). Grooming was defined as either a crouching posture over the pup together with head movements indicating licking of the pup, or olfactory inspections of the pup together with the forepaws of the experimental mouse being in touch with the pup.

Grooming score was quantified based on the time the female spent grooming the pup compared to the time spent in the pup zone in presence of the pup (express in percentage). Nest building was defined as nesting material collection and placement in order to reduce its dispersion across the arena. We calculate the time spent nesting for each mouse and we normalize it based on the total duration of the session. The quality of the nest was assessed at the end of the session following previously published score scale. Briefly, a score of 20% was given when the shredded paper remained scattered throughout the cage; 40% was assessed when some of the material was constructed into a nest; 60% when a noticeable nest was constructed, but several pieces were still scattered; 80% when almost all the material was used for the nest and 100% when all material was used to make an identifiable and organized nest. The nesting score was calculated as the average of the time spent nesting and the quality of the nest.

Retrieval episodes were split in 4 subsequent phases: Approach was defined as the first step toward the pup from the point farthest away from the pup. Interaction was defined as close contact to any parts of the body of the pup by the frontal end of the female. Retrieval onset was defined as the moment the female opened her jaw and made contact with the skin of the pup. Retrieval offset was scored as the moment when the female dropped the pup in the nest. Object interaction was defined as nose contact with any part of the object. Conspecific interaction was defined as close contact with any part of the conspecific. Regarding photometry and endoscope recordings, for object, conspecific, pup interaction (without retrieval), nest building and grooming only events separated by at least 10 seconds were included in the analysis. Most behavioural annotation was not done blindly. For a subset of videos, we

compared the annotations done by an annotator blind to the experimental conditions and one that was not, founding high consistency.

Fiber photometry recordings

Fiber photometry measurements were carried out by the ChiSquare X^2-200 system (ChiSquare Biomaging, Brookline, MA). Briefly, blue light from a 473-nm picosecond-pulsed laser (at 50 MHz; pulse width ~80 ps FWHM) was delivered via a single mode fiber. Fluorescence emission from the tissue was collected by a multimode fiber with a sample frequency of 100Hz. The single mode and multimode fibers were arranged side by side in a ferrule that is connected to a detachable multimode fiber implant. The emitted photons collected through the multimode fiber pass through a bandpass filter (FF01-550/88, Semrock) to a single-photon detector. Photons were recorded by the time-correlated single photon counting (TCSPC) module (SPC-130EM, Becker and Hickl, GmbH, Berlin, Germany) in the ChiSquare X^2-200 system.

Microendoscopic calcium imaging

All calcium imaging was recorded at 20 frames per second, 200-ms exposure time, and 10%–40% LED power (0.4-0.9mW at the objective, 475nm) using a miniature microscope from Inscopix (nVista). Calcium recording files were down-sampled (spatial binning factor of 4) to reduce processing time and file size, filtered, corrected for rigid brain movement and the ΔF/F0 was calculated using as F0 the average fluorescence for all the video (Inscopix, IDP). Individual component analysis and principal component analysis (ICA/PCA) applications were used to identify individual cells and to extract their respective calcium traces. In addition, to compare ROI detections and relative traces obtained with the PCA/ICA we also performed constrained non-negative matrix factorization for endoscopic data (CNMF-E) for a subset of data. Briefly, we denoised, deconvolved, and demixed calcium-imaging dynamics (https://www.github.com/zhoupc/cnmf_e). Calcium imaging frames were initially pre-processed in Mosaic (Inscopix) for motion correction. We use a Gaussian kernel width 4 μm, maximum soma diameter 16 μm, minimum local correlation 0.8, minimum peak-to-noise ratio 8 and merging threshold was set to 0.65 for optimal discrimination of temporal and spatial overlap.

To determine the putative cell location in the LHb we proceed as follow: we registered each field of view (FOV) of GCaMP6f-expressing neurons and aligned it to the GRIN lens borders visualized on post-hoc fixed brain sections (Fig. 2g and Extended Data Fig. 3a and 4a). We then annotated the active neurons within individual FOVs to build cell masks, and subsequently we overlapped them, GRIN lenses borders and LHb anatomy from all mice.

Analysis of calcium signal

Photometric signal as well as miniscope PCA/ICA derived traces were smoothed (constant time factor, 0.1 s) and further processed according to the trials using Spike2 software (Cambridge Electronic Design). We obtained an average peri-event time histogram (PETH) trace aligned to the events (2-7 s prior and 2-7 s after a given event). For the pup retrieval phases we z-scored each trials in reference to their baseline (7

s prior to the approach). For nesting, grooming events we used as reference the average and SD of the relative recording/movie. For conspecific, object and airpuff the z-score was calculated in relation to the 2s prior of the event.

Photometry: The duration of the fluorescent transient (Fig 1e) was calculated as follow: first we bin the z-score (10 Hz) around the retrieval episode (-10 to + 40 seconds). Then we consider the transient starting at the first bin higher than 2-score and terminated when we encounter more than 5 consecutive bins not fitting the criteria.

Single trial quantification was obtained, by the z-score of the 0.5 first seconds after the events except the retrieval offset (we plotted the last 0.5 s cause the slow decay of the GCaMP6).

Endoscope: for the single cell reliability analysis, we analyzed the fluorescence Ca2+ signals of individual trials after a given event, using 1 s time span. We consider a cell responding during a trial if the signal was higher than 2 z-score. The reliability account for the number of trial where the cell respond divided the total number of trials (express as percentage). Average amplitude calculated at the same time-span was obtained for each cell recorded.

The response was defined as “specific” if the activity was reaching 5 z-score for a mean duration of 0.3 sec during a window of 4sec centered onto a given event (Fig 4g).

Clustering and decoding

For clustering neurons based on their average responses around all the retrieval phases, grooming and nest building events we followed a similar general procedure as in Lecca et al. (2020). Briefly, we first calculated the average perievent time histogram (PETH) for each neuron around each action by averaging all trials. Due to the variability in duration of retrieval episode, and therefore to avoid signal contamination from subsequent phases, we considered the average signal in a time window from 0.0 s to 1.0 s for each episode. These time windows were treated as features of the response of a neuron. This feature space was then reduced in dimensionality using principal components analysis. The number of principal components to keep was decided based on the bend in the scree plot. A spectral clustering algorithm along with optimal selection of number of clusters using silhouette scores was used on the principal component scores to test for presence of clusters. The number of clusters was chosen by maximizing the silhouette score. Once cluster identities were assigned, all PETHs were recalculated using the activity from −7 s to +2 s for approach, -2 s to +2 s for interaction and retrieval onset, -2 s to +7 for retrieval offset and from -5 s to +5 s for nest building and grooming behaviours.

Decoding approach was used to create a model and attempt to reveal whether particular information is representative in calcium neuronal activity to predict category labels of behavioural events scored previously. A shuffle category was added by randomly permuting calcium neuronal activity from equally distributed number of trials of the different category of behavioural events. Based on PETHs of calcium activity from recorded neurons around a time window from -2sec to +2sec surrounding each event,

multiple features were analyzed. To obtain these features, the probability distribution of amplitude of activity and duration (expressed in ratio of total time) of significant increased activity (>1.96 z-score) were computed and the following properties of each distribution were extracted: mean, median, coefficient of variation, skewness and kurtosis. The number of time bout as well as the total duration in significant increased activity was also computed. The features were normalized by using z-score and by rescaling the values. Then the dimensionality was reduced by using UMAP technique for visualization or a classifier was built by using k-nearest neighbor approach based on BNST-receiving LHb calcium neuronal activity with euclidean distance metric and a 5-fold cross-validation. By using this classifier model, the posterior probability that the neuronal activity is associated with each category of scored behaviour was then calculated. The decoding performance for each neuron during each behaviour was normalized by dividing it with the average posterior probability of the cluster 1 LHb neurons previously defined for corresponding behavioural category.

In vitro recordings

Virgin female mice were anaesthetized with ketamine (150 mg.kg-1) and xylazine (100 mg.kg-1) (Veterinary office University of Lausanne) and brains were rapidly extracted. Coronal slices (250 micrometers) of LHb and BNST were sectioned using a vibratome (Campden instruments), while immersed in an ice-cold solution, bubbled with 95% O2 and 5% CO2 and containing (in mM): choline chloride (110), glucose (25), NaHCO3 (25), MgCl2 (7), ascorbic acid (11.6), sodium pyruvate (3.1), KCl (2.5), NaH2PO4 (1.25), and CaCl2 (0.5). The low temperature and high level of magnesium limit the release of neurotransmitters and cell death. Slices were then incubated for 5 mins at 34°C in a solution of identical composition before being stored at room temperature in artificial cerebrospinal fluid (ACSF) containing (in mM): NaCl (124); NaHCO3 (26.2); glucose (11); KCl (2.5); CaCl2 (2.5); MgCl2 (1.3); and NaH2PO4 (1), for an hour prior recording. This solution allows us to preserve the integrity of the neurons throughout the day, by supplying oxygen and maintaining osmolarity and pH at biological levels.Whole cell voltage clamp recordings of LHb neurons were obtained using borosilicate glass pipettes (Phymep; impedance: 2.5-4 MΩ) filled with Cs-based intracellular solution containing (in mM): cesium methanesulfonate 120, CsCl 10, HEPES 10, EGTA 10, creatine phosphate 5; Na2ATP 4; Na3GTP 0.4. The bath solution (ACSF) was kept at 31°C with a flow rate of 2mL/min.

During the recordings, electrical signal was filtered (5 kHz) and digitized (10 kHz) using MultiClamp 200B (Molecular Devices). Data acquisition was performed with Igor Pro and NIDAQ tools (Wave Metrics). Access resistance was continuously monitored with a voltage step of −4 mV (0.1 Hz). Post synaptic currents were evoked with a LED coupled to Master-8 (AMPI) and an Olympus-BX51 microscope, delivering pulses of blue light (473 nm, 5 mW, 1-10 ms duration). Evoked excitatory and inhibitory post synaptic currents were recorded at -60mV and +5 mV, respectively. After the recordings, slices were kept overnight in PFA to verify the injection site (BNST) and the presence of fibers (LHb) using an epi-fluorescent microscope (Zeiss).

In vivo recordings

Mice, previously injected with ChR2 in the BNST were anaesthetized using isoflurane (Induction: 4%; maintenance: 1–1.5%) and placed in the stereotaxic apparatus (Kopf, Germany). Their body temperature was maintained at 36 ± 1°C using a feedback-controlled heating pad (CMA 450 Temperature controller, Phymep). The scalp was retracted, and one burr hole was drilled above the LHb (AP: −1.3 to −1.6 mm, L: 0.35–0.5 mm, V: −2.3 to −3.2 mm) for the placement of a recording optrode. Single-unit activity was recorded extracellularly using glass micropipettes filled with 2% Chicago sky blue dissolved in 0.5 M sodium acetate (impedance 5–15 MΩ). Signal was filtered (band-pass 500–5000 Hz), pre-amplified (DAM80, WPI, Germany), amplified (Neurolog System, Digitimer, UK) and displayed on a digital storage oscilloscope (OX 530, Metrix, USA). Experiments were sampled on- and offline by a computer connected to CED Power 1401 laboratory interface (Cambridge Electronic Design, Cambridge, UK) running the Spike2 software (Cambridge Electronic Design).

Single units were isolated and the spontaneous activity was recorded for a minimum of 3 min before assessing their response to BNST terminal optogenetic stimulation (15 trials, 40 Hz, 1 s, 473 nm, 8 mW). Peristimulus time histograms (PSTHs) and raster plots were built using 100 ms bin width. A cell was considered excited when the mean number of action potentials/bin in at least one of the five epochs (200 ms per epoch) after the light onset was higher than the baseline (the average number of action potentials/bin in the 2-s period before the light onset) plus two times the Standard Deviation (SD).

Inhibition was assessed if the mean count during the light period (1 s) dropped at least 35% below average baseline

Each BNST-excited cell was also tested for its response to repetitive (every 5 s) shocks (0.5 s, 1 mA) delivered to the hind paw contralateral to the recording side. PSTH was built using 10 ms bin width. Excitation or inhibition to Fs were assessed as previously reported (Congiu et al., 2019).

At the end of each experiment, mice were euthanized (overdose of isoflurane prior to killing) and the electrode placement was determined with an iontophoretic deposit of pontamine sky blue dye (1 mA, continuous current for 5 min). Brains were then rapidly removed and fixed in 4% paraformaldehyde solution. The position of the electrodes was identified with a microscope in coronal sections (60 µm). Only recordings in the correct area were considered for analysis.

Optogenetics experiments

After stereotaxic surgeries, the viruses were allowed to incubate for 4–7 weeks before behavioural testing. A ferrule patch cord was coupled to the ferrule fiber implanted in the subject mouse using a sleeve (Thorlabs). Optical fibers were connected to a 473 nm blue laser, (power 12 mW, Shangai Dream lasers technology) or a 638 nm red laser (power 4mW, MatchBox series, Integrated Optics, US). For the ChR2 experiment, the laser was remotely activated (473 nm, 40 Hz, 10 ms pulse duration) by the experimenter at the onset of interaction and turn off at the exit of the pup zone. This experiment was a “within animal” design: we alternate trial with light-paired with pup interaction in the pup zone with period (max 5 minutes) where the light was always off. For the JAWS experiments, for each trial the laser was activated

(638 nm, continuously) and inactivated via the I/O box each time the females entered or quit the pup zone, respectively.

Single-nucleus RNA-seq

Nuclei preparation and FAC-sorting: Three virgin males, three virgin females and three mothers were sacrificed and brains were extracted in ice-cold oxygenated ACSF (containing (in mM): NaCl (124); NaHCO3 (26.2); glucose (11); KCl (2.5); CaCl2 (2.5); MgCl2 (1.3); and NaH2PO4 (1)). Each brain was then sectioned coronally at 1250 µm using a vibrating microtome (Campden Instruments). The lateral habenula was micro-dissected under a stereomicroscope, incubated for 5 min in 500 µl chilled 0.1X NP40 Lysis Buffer (Tris-HCL pH 7.4 10mM, NaCl 10mM, MgCL2 3mM, Tween-20 0.1%, NP40 0.1%, BSA 1%, DTT 1mM and RNase inhibitor), mechanically dissociated using a pellet pestle (15 goings and ongoings) and finally incubated on ice for 5 min. The suspension was then washed with 500 µL chilled wash buffer (Tris-HCL pH 7.4 10mM, NaCl 10mM, MgCL2 3mM, Tween-20 0.1%, BSA 1%, DTT 1mM, RNase inhibitor). Nuclei were then filtered through a 30-µm cell strainer, centrifuged (1000g, 10 minutes at 4°C) and resuspended in 500 µL of FACS buffer (Tris-HCL pH 7.4 10mM, NaCl 10mM, MgCL2 3mM, BSA 1%, DTT 1mM, RNase inhibitor). Positive GFP nuclei were sorted using a BD FACS Aria II flow cytometer (BD Biosciences) and collected in ice-cold FACS buffer.

Single-nuclei RNA capture and sequencing and quality controls: After sorting, nuclei were counted and immediately processed according to the 10X Chromium protocol. Briefly, an appropriate volume of each cell suspension containing 1000 cells from the three different conditions was combined with 10X Chromium reagent mix and samples were loaded into three separate lanes. Nuclei capture, lysis, mRNA reverse transcription, cDNA amplification and libraries were performed following 10X Genomics Chromium dual indexing Single Cell 3' V3.1 reagent kit instructions. Libraries were then multiplexed and sequenced according manufacture recommendations with paired-end reads using a HiSeq4000 platform (Illumina) with an expected depth of 250’000 reads per single nuclei. All the sequencing experiments were performed within the Genomics Core Facility of the University of Lausanne. Alignment of sequenced reads to the mouse genome (GRCm38) and filtered gene–barcode matrices were realized by running Cell Ranger Single-Cell Software Suite v5.0.1 (10X Genomics). The cell ranger count function was used to generate filtered gene/cell expression UMI corrected matrices by selecting probable nuclei and removing empty lipid droplets (219 nuclei for “virgin females” condition, 225 nuclei for “virgin males” condition and 223 nuclei for “mothers”). To filter only high-quality cells, we applied selection based on mitochondrial genes percentage (>10 %) and number of genes per cell (>500 genes). After applying these filters, 196 nuclei for “virgin females” condition, 205 nuclei for “virgin males” condition and 202 nuclei for “mothers” condition were kept for further analysis.

Single cell RNA sequencing Habenula database: For Wallace et al., dataset, count matrix was downloaded from Harvard database website https://doi.org/10.7910/DVN/2VFWF6, and metadata were kindly provided by the authors (11878 cells). For Hashikawa et al., datasets, count matrix was downloaded from

GEO under accession number GSE137478 and metadata were also kindly provided by the authors (7506 cells).

Data integration and visualization: To generate reference habenula atlas, we applied data integration procedure from Seurat and identified shared sources of variation between Wallace and Hashikawa datasets. Briefly, each dataset was normalized and scale using SCTransform procedure from seurat. We then identified common features and used the “FindIntegrationAnchors” function with using for normalization method “SCT” and default parameters. We then performed the integration using the “IntegrateData” function and default parameters. For UMAP visualization, dimensionality reduction was performed using standard function in Seurat. To identify BNST-receiving LHb neurons clusters, we first adopted a graph-based clustering approach using “FindClusters” function from Seurat with a resolution of 0.4. We then use the Transfer Data function from Seurat to automatically annotate each cluster base on the reference habenula atlas annotation.

Differential expression analysis: Differentially expressed genes were identified based on their weight, resulting from differential pairwise expression analysis using Seurat “FindAllMarkers” function with default parameters (expect only.pos = TRUE, min.pct = 0.2, logfc.threshold = 0.5, and their p-value lower than 0.05). The identified gene candidates for each condition were interrogated for statistically significant gene ontologies using GSEA (http://software.broadinstitute.org/gsea/index.jsp). As background universe gene list for the Gene Ontology (GO) term analysis, we used a total of 32885 genes corresponding to all genes detected. For gene ontology enrichment, the top 20 “biological processes” or specific term enrichment such as “GABA” or “Hormone” were filtered using a false discovery rate (FDR)-corrected P value lower than 0.1 as a cutoff. Gene ontology filtered for “GABA” term analysis of gene candidates across biological processes. The string database platform (http://string-db.org) was used to determine the protein-protein interactions.

Statistics

All statistical analyses were conducted using Prism (v.9, GraphPad). Statistical tests used in this study include paired and unpaired t-test, Wilcoxon matched-pairs tests, Chi Square test, one-way and two-way analysis of variance (ANOVA). When parametric tests were used, data normality was confirmed using the Shapiro–Walk normality test. P values were corrected for multiple comparisons when necessary. The bar plots show the mean ± s.e.m. In the box plots, the centre lines indicate the median, the box limits indicate the upper and lower quantiles. The significance threshold was held at $\alpha = 0.05$. All behavioural, imaging and optogenetics experiments were replicated in multiple batches of animals with similar results. Sample sizes were not predetermined using statistical methods. Experiments were randomized whenever possible. Experimenters were not blind to the experimental group.

Declarations

Acknowledgements

We thank C. Lüscher, D. Jabaudon, B. Benedetti, M.A. Diana, F.J. Meye and all the members of the Mameli laboratory for comments on the manuscript. We thank M. Gotz and R. Bocchi for the kind gift of the KASH viral construct, and the animal caregivers team of the Department of Fundamental Neuroscience. This work was supported by the Swiss National Funds 31003A and Vaud Canton to M.M., the NARSAD Young Investigator to S.L..

Author contributions

S.L. and M.M. conceptualized the project. S.L. conducted and analyzed behaviours and in vivo calcium imaging with the help of L. Restivo, L. Royon and M.C.. N.M. and L.T. performed and analyzed single-cell sequencing data. M.C., B.G. and C.B. supported S.L. in the analysis of imaging data. M.M. and S.L. wrote the manuscript with the help of all authors.

Supplementary Information is available for this paper.

Data availability

The data that support the findings of this study are available from the corresponding author upon reasonable request.

Code availability

The code used for analysis (Python) is available from the corresponding author upon reasonable request.

Correspondence and requests for materials should be addressed to Manuel Mameli.

Supplementary Tables

Supplementary Tables 1 and 2 are not available with this version

Figures

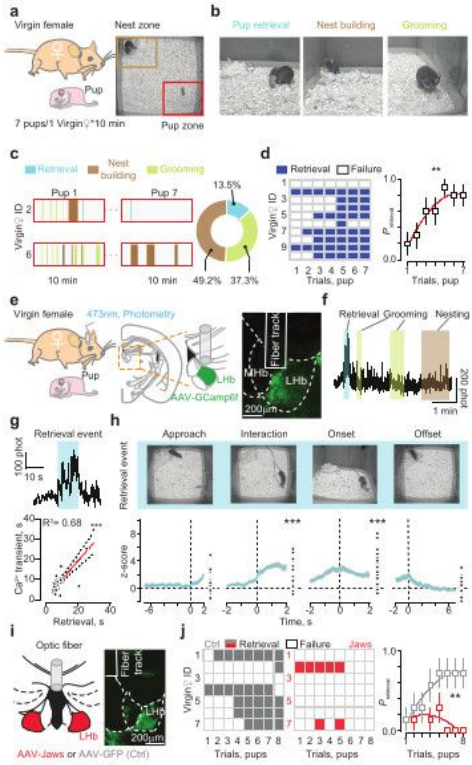

Fig. 1, Lecca et al.,

Figure 1

LHb neuronal dynamics during parental behaviours. a, Experimental setting where each virgin female mouse underwent 7 trials. Each trial consists in exposing a pup (pup zone, red square) for a maximum of 10 minutes. Retrieval absence within 10 minutes scores as failure. b, Video snapshots capturing a virgin female mouse during pup retrieval, nest building and grooming. c, Representative schematic reporting single trial behavioural events of two virgin female mice. Colors denote the three different behaviours

scored. Pie-chart summarizes the total bouts of events scored for each behaviour (n_{mice}= 10, $n_{retrieval}$= 42, $n_{nest\ building}$= 153, $n_{grooming}$= 113). d, Binary map depicting retrievals (blue) and failures (white) for each mouse and retrieval probability with sigmoidal fit (n_{trials}= 7; $F_{6,54}$=7.23, **p=0.0014, one-way ANOVA RM). e, Schematic of the photometric calcium recordings and representative coronal section showing neuronal GCaMP6f transduction with fiber track in the LHb. f, LHb neuronal activity during the expression of parental behaviours (colored squares). g, Magnification of a single pup-retrieval-driven transient (blue) and (bottom) correlation between retrieval and calcium transient duration (n_{mice}= 5, n_{trials}= 28, ***p<0.0001, Pearson r). h, Extracted video frames for subsequent phases of retrieval episode and relative LHb fluorescent z-score ($F_{4,108}$= 25, ***p<0.0001, One Way ANOVA RM and Dunnett test). i, Schematic of LHb optogenetic inhibition and representative coronal section with Jaws transduction in the LHb and fiber track. Continuous red light (638 nm) was triggered from a laser via a close-loop feedback control system locked with the entrance of the virgin female mouse in the pup zone. j, Binary maps and retrieval probability in Ctrl (in gray) and Jaws-injected virgin female mice (in red). Ctrl vs Jaws, n_{mice}= 7; n_{trials}=8; $F_{7,84}$= 3.49, **p=0.0024, Two Way ANOVA RM. Data are represented as single plots or means with SEM.

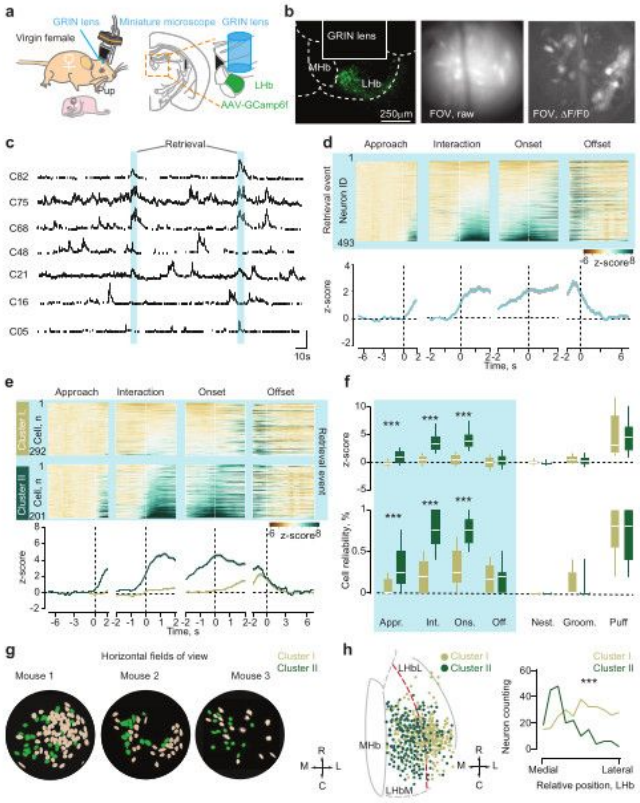

Fig. 2, Lecca et al.,

Figure 2

LHb clusters differentially signal pup-retrieval events. a, Microendoscopic imaging in a freely moving virgin female mouse. b, GRIN lens placement in the LHb and GCaMP6f neuronal expression, field of view (FOV, bright field) and maximum intensity projection of the ΔF/F0 for the same FOV. c, Sample traces of 7 LHb neurons in a virgin female mouse (blue reflects retrieval events). d, Heatmap of z-scores in single neurons time-locked with the different phases of pup retrieval sorted by lower responsive cells at the

interaction. Bottom. Average z-score timeline for all neurons (n_{mice}= 7, n_{cells}= 492). e, Clustering analysis heatmaps revealing 2 segregated clusters, and their relative average z-score during the behaviour (n_{cells}. Cluster 1= 292; Cluster 2= 201). f, Top. Boxplots showing the cell mean amplitude (z-score) during each event for Cluster 1 and cluster 2. (n_{mice}= 7. n_{cells}: Cluster 1= 292; Cluster 2= 201; Pup retrieval: Cluster x phase, $F_{3,1473}$ = 271.8, ***p<0.0001 Two Way ANOVA RM and Sidak's multiple comparison test). Bottom. Boxplot reports single cell reliability (%) for the same events (Pup retrieval: Cluster x phase: $F_{3,1473}$ = 166.7, ***p<0.0001 Two Way ANOVA RM and Sidak's multiple comparison test). g, Maximal projections in FOV from 3 representative mice with colors matching cluster identity. h, Anatomical reconstruction-based global cell projection and relative quantification illustrating LHb spatial distribution in the medio-lateral axis for Cluster I and II neurons (X^2_{10} = 96.85, ***p<0.0001, Chi Square test). Data are represented as means with SEM.

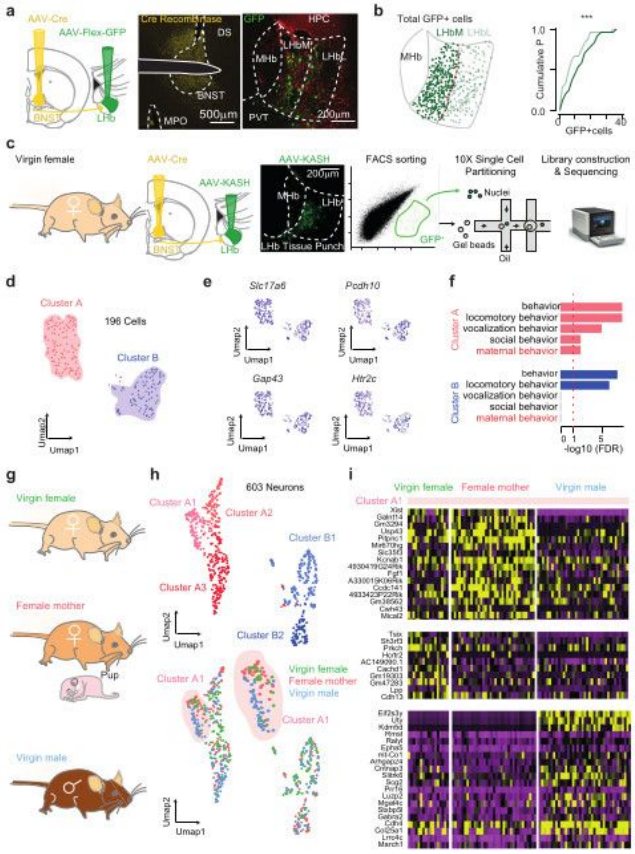

Fig. 3, Lecca et al.

Figure 3

A molecular signature for parenting in ^{BNST}LHb neurons. a, Intersectional approach and representative images showing Cre recombinase labelling in the BNST, together with GFP and NeuN labelling in the LHb. b, Anatomical distribution of GFP+ ^{BNST}LHb cells and relative cumulative probability plot (n_{mice}= 4, $n_{replicata/mouse}$= 6; n_{GFP+} = 522, ***p<0.0001, Wilcoxon matched-pairs test). c, Schematic representation of

the experimental paradigm. Viral injections were performed on virgin females using an adeno-associated viruses (rAAV1-hSyn1-Cre) targeting BNST neurons and an adeno-associated virus (AAV-Flex-KASH-GFP) to express nuclear GFP in LHb Cre-expressing cells. LHb microdissections were dissociated into single-nucleus suspensions and GFP+ nuclei were FACS-sorted for sequencing using the droplet-based 10x Genomics system. d, UMAP representation of single-nuclei RNA sequencing revealing BNST-receiving LHb neurons transcriptional cluster organization. e, Combinatorial expression of LHb specific genes. f, Gene ontology analysis of gene candidates across biological processes filtered for “behaviour” term are highlighted. The red dashed line indicates the threshold for significant enrichment. g, Representative drawings reporting the three experimental groups. h, UMAP representations of single-nuclei RNA sequencing revealing BNST-receiving LHb neurons cluster organization in virgin females, mothers and virgin males. i, Heatmap representation of significantly differentially expressed genes for cluster A1 between virgin females, mothers and virgin males.

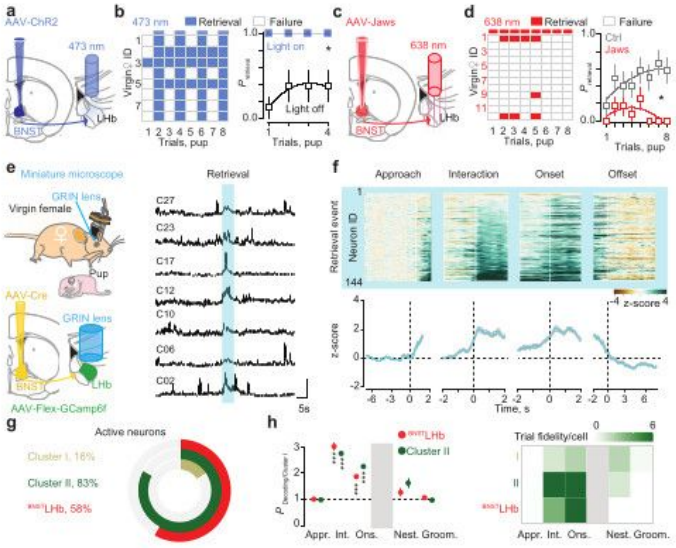

Fig. 4, Lecca et al.,

Figure 4

^{BNST}LHb neurons track pup-retrieval. a, Schematic of the BNST-LHb activation experiment on pup retrieval. b, Binary map and probability graph reporting the comparison within mice injected with ChR2 in the BNST on pup retrieval during light-paired vs not-light paired trials (n_{mice}= 8, nt_{rials}= 4 vs 4; light vs no light, $F_{3,42}$= 2.43, *p=0.045, Two Way ANOVA RM). c, Schematic of the BNST-LHb inhibition experiment on pup retrieval test. d, Binary maps and graph depicting respectively single mouse performance and

probability to retrieve across trials in ctrl (gray) and Jaws-injected females (red). Ctrl vs Jaws, n_{mice}= 12; n_{trials}=8; $F_{7,154}$ = 2.431 *p=0.0027, Two Way ANOVA RM. e, Microendoscopic imaging from ^{BNST}LHb in a freely moving virgin female mouse sample FOV with maximum intensity projection of the ΔF/F0. f, Heatmap of the single neuron z-score time-locked with phases of pup retrieval and sorted from the lower responsive cells to interaction (n_{mice}= 4, n_{cells}= 144). Bottom. Average z-score timeline for the ^{BNST}LHb population during pup-retrieval. g, Pie-chart reporting fraction of neurons for each cluster showing specific response to interaction and retrieval onset. h, Single-cell decoding probability for Cluster II and ^{BNST}LHb neurons express as ratio with Cluster I average (***p<0.0001, Brown Forsythe and Welch ANOVA test). Bottom. Heatmap reporting the fidelity of single trial for each cell (Cluster I vs Cluster II vs ^{BNST}LHb). Data are represented as means with SEM.

Supplementary Files

This is a list of supplementary files associated with this preprint. Click to download.

- 20220317ExtendeddataFig.1Leccaetal.pdf
- 20220317ExtendedDataFig.2Leccaetal.pdf
- 20220317ExtendedDataFig.3Leccaetal.pdf
- 20220317ExtendedDataFig.4Leccaetal.pdf
- 20220317ExtendedDataFig.5Leccaetal.pdf
- 20220317ExtendedDataFig.6Leccaetal.pdf
- 20220317ExtendedDataFig.7Leccaetal.pdf
- 20220317ExtendedDataFig.8Leccaetal.pdf
- 20220317ExtendedDataFig.9Leccaetal.pdf
- 20220317ExtendedDataFig.10Leccaetal.pdf
- SupplementaryVideo1.mp4
- SupplementaryVideo2.mp4
- SupplementaryVideo3.mp4